Journal of Applied Electrochemistry **33**: 607–612, 2003.

Structural and electrochemical characterization of mechanochemically synthesized calcium zincate as rechargeable anodic materials

X-M. ZHU, H-X. YANG*, X-P. AI, J-X. YU and Y-L. CAO
Department of Chemistry, Wuhan University, China 430072
*(*author for correspondence, fax: +86 27 87884476, e-mail: ece2000@263.net)*

Received 20 August 2002; accepted in revised form 24 March 2003

Key words: anodic material, calcium zincate, cycling properties, mechanical milling, XRD analysis

Abstract

Hydrated calcium zincate was synthesized by mechanical ball milling of ZnO and $Ca(OH)_2$ in water at room temperature. The structural and electrochemical properties of this material used as rechargeable anodic material were examined by microelectrode voltammetry, charge–discharge measurements and structural analysis. The results showed that during mechanical milling, ZnO, $Ca(OH)_2$ and H_2O reacted rapidly to form $Ca[Zn(OH)_3]_2 \cdot 2H_2O$ which was subsequently transformed to a stable structure $CaZn_2(OH)_6 \cdot 2H_2O$. Since this composite oxide has lower solubility in KOH solution (<35 wt %) and better electrochemical reversibility than ZnO-based negative materials, the zinc anodes using this material can overcome the problems of shape changes and dendritc formation, and therefore exhibit improved cycling life.

1. Introduction

Secondary batteries using zinc anodes and alkaline electrolytes have received considerable research attention because of their high energy density, low cost and environmental friendliness. One of the major problems limiting commercial development of these batteries is the poor cycleability of the zinc anodes. During charge–discharge cycling, the electrochemical dissolution and deposition of zinc proceed non-uniformly on the electrode surface, resulting in shape change, dendrite formation and electrode densification. These detrimental effects can severely degrade the electrode performances or rapidly cause cell failure. To solve these problems, many attempts have been made to improve zinc utilization and cycleability by addition of various metal oxides and hydroxides [1–5], modification of electrolyte composition and properties [6–10], applying physical techniques such as pulse charging [11], improvement of separators [12] and vibrating electrodes [13]. These techniques can improve the cycling properties of zinc anodes to some extent, but it is still difficult to meet the requirements of most practical applications.

Another approach to solve these problems is to use insoluble composite oxides of zinc instead of zinc oxide as electroactive materials. Among the composite oxides of zinc, calcium zincate seems to be a promising candidate because of its electrochemical reversibility and structural stability. In a previous paper, we reported the electrochemical properties of calcium zincate synthesized by a chemical coprecipitation method [14]. In the present work, we report a simple preparation method of calcium zincate by mechanical ball milling and describe the structural and electrochemical properties of the material used as rechargeable zinc anode.

2. Experimental details

2.1. *Preparation and structural characterization*

Calcium zincate was prepared by mechanical ball milling of ZnO and $Ca(OH)_2$ in water medium. The starting reagents was weighed, mixed and put into an agate pot together with 10 mm diameter agate balls. The weight ratio of the starting materials to milling balls was selected as 1:4. The milling pot was tightly sealed and set in a planetary ball miller. Usually the ball milling treatment was carried out with rotation speed of 70 rpm for 2 h at room temperature. After ball milling, the slurry product was filtered, washed with distilled water and then dried at 50–70 °C.

To characterize the chemical changes during ball milling, X-ray diffraction measurements (XRD) were used to identify the crystalline phases of the samples at various milling periods. The samples were taken from the milling pot at given periods and then quickly filtered for immediate XRD analysis. XRD measurements were performed on a Shimadzu lab XRD diffractometer with CuK_α source. Thermogravimetric analysis (TGA) and differential scanning calorimetry (DSC) were also used to determine the changes in the chemical composition of

the composite oxide during the formation of calcium zincate. TGA and DSC analysis were carried out in N_2 atmosphere with flow rate of 100 mL min^{-1}, and scan rate of 10 °C min^{-1}.

At room temperature, the solubility of calcium zincate in alkaline solution was measured by complexometric titration experiments. The complexometric titration was carried out in 20 wt % hexamethylene tetramine buffer solutions using 0.1 mol L^{-1} EDTA solution as complexant and 0.2 wt % xylenol orange as indicator.

2.2. *Electrochemical measurements*

The cyclic voltammetric behaviour of calcium zincate was examined by a microelectrode technique. The working microelectrode was made by filling fine powders of calcium zincate into a microcavity at the tip of a Pt microdisc electrode [15]. A large nickel sheet served as counter electrode and a HgO/Hg electrode was used as reference electrode.

The charge–discharge properties of calcium zincate were examined on simulated cells of anode-limited design. A typical experimental cell consisted of a calcium zincate anode sandwiched by two pieces of sintered nickel cathodes. The anode was prepared by mixing 85 wt % calcium zincate powders, 1 wt % cellulose, 2 wt % PbO, 10 wt % acetylene black and 2 wt % PTFE (in diluted emulsion) into paste, then rolling the pasted mixture into about 0.1 mm thick electrode sheet, and finally pressing the electrode sheet onto expanded copper net. The electrolyte was 20 wt % KOH solution with addition of 15 g L^{-1} LiOH. Charge–discharge cycling was carried out at constant current and controlled by cell voltage between +2.05 V and +1.60 V, which corresponded to a 100% discharge depth of the anode. To identify the changes in crystalline structure and surface morphology of cycled electrodes, the test cells at various cycling periods were disassembled and the anodes were taken out for XRD and SEM analysis.

3. Results and discussions

3.1. *Chemical reactions in the mechanical synthesis*

Figure 1 shows XRD diffractograms of the mixture of $Ca(OH)_2$, ZnO and H_2O obtained at various periods of ball milling. At the beginning of mechanical milling, XRD data of the sample showed a combined pattern characteristic of ZnO ($d = 2.48$, 2.81 and 2.60) and $Ca(OH)_2$ ($d = 2.62$, 4.89 and 1.92) [16]. With increasing milling time, the characteristic diffraction peaks of ZnO and $Ca(OH)_2$ decreased gradually and disappeared completely after 120 min of milling. At the same time, new XRD peaks appeared at $d = 3.12$ and $d = 6.25$, and their relative intensities quickly increased with milling time. By comparison with standard XRD data [17], the diffraction peaks could

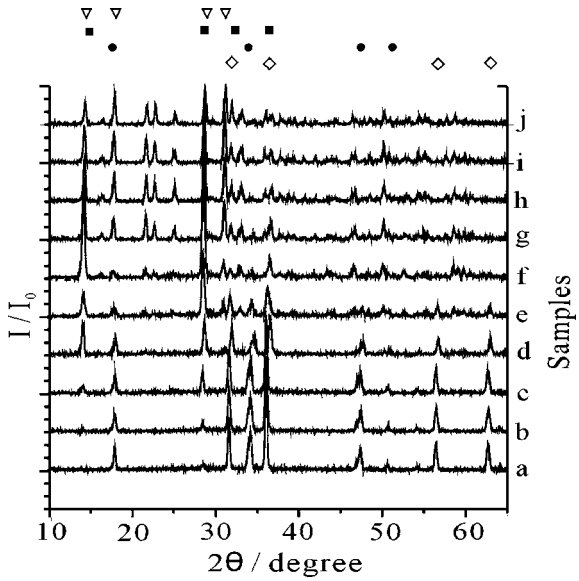

Fig. 1. X-ray diffractograms of the mixture of $Ca(OH)_2$, ZnO and H_2O at various periods of ball milling: (a) 0, (b) 30, (c) 60, (d) 90 and (e) 120 min, also (f) 24, (g) 48, (h) 72, (i) 96 and (j) 120 h. Key: (●) $Ca(OH)_2$, (◇) ZnO, (■) $Ca[Zn(OH)_3]_2 \cdot 2H_2O$ and (▽) $CaZn_2(OH)_6 \cdot H_2O$.

be attributed to $Ca[Zn(OH)_3]_2 \cdot 2H_2O$, suggesting the formation of hydrated calcium zincate during the mechanical milling. When the ball milling continued, a number of peaks appeared at $d = 5.47$, 5.01, 4.15, 3.96, 3.61 and 2.82, and the relative intensities of the peaks gradually increased along with ball milling treatment, while the $d = 3.12$ and $d = 6.25$ peaks of $Ca[Zn(OH)_3]_2 \cdot 2H_2O$ slowly diminished, implying a structural change in the crystalline phase of the composite oxides. It is known that hydrated calcium zincate exists in two types of crystalline structures: $Ca[Zn(OH)_3]_2 \cdot 2H_2O$ and $CaZn_2(OH)_6 \cdot 2H_2O$, both of which belong to the Monoclinic crystal system with $P2_1/c$ space symmetry. The only difference in the two types of crystalline structures appears in the β value of the crystal cells. The crystal cell parameters of $Ca[Zn(OH)_3]_2 \cdot 2H_2O$ are $a_0 = 6.384$, $b_0 = 10.967$, $c_0 = 5.759$ and $\beta = 101.92°$, while $CaZn_2(OH)_6 \cdot 2H_2O$ has crystal cell parameters of $a_0 = 6.384$, $b_0 = 10.977$, $c_0 = 5.756$ and $\beta = 78.02°$ [17]. However, the XRD features of the two crystalline phases are quite different, $Ca[Zn(OH)_3]_2 \cdot 2H_2O$ give the characteristic XRD peaks at $d = 3.12$, 6.25 and 2.88, but the characteristic XRD bands of $CaZn_2(OH)_6 \cdot 2H_2O$ are at $d = 2.88$, 5.01 and 3.12 [17]. By comparison of the XRD lines in Figure 1 with the standard XRD data, it could be concluded that during the ball milling, ZnO and $Ca(OH)_2$ react quite rapidly to form $Ca[Zn(OH)_3]_2 \cdot 2H_2O$ which transforms gradually to $CaZn_2(OH)_6 \cdot 2H_2O$ at prolonged milling treatment.

Thermal analysis of calcium zincate also agrees with the XRD results, Figure 2 gives TGA and DSC curves of the calcium zincate synthesized by ball milling. In DSC curves of calcium zincate, there were four endo-

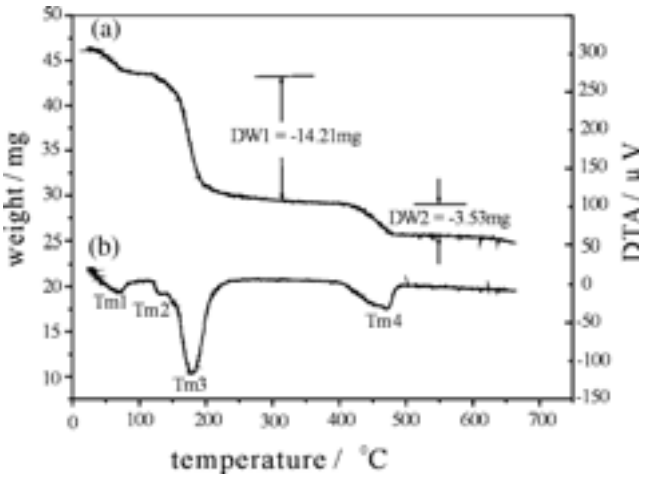

Fig. 2. TGA (a) and DSC (b) curves of calcium zincate obtained by ball milling.

thermic bands at about 70, 120, 180 and 450 °C. The first two weak bands at 70 and 120 °C are usually observed for hydrated oxides and are considered here to result from the evaporation of residual solvent water and the loss of hydrated water in the sample respectively. The strong endothermic band at 180 °C corresponds to the dehydration of $Zn(OH)_2$ to form ZnO as confirmed by parallel DSC analysis of $Zn(OH)_2$. The DSC band at 450 °C was due to the dehydration of $Ca(OH)_2$. Since the loss of hydrated water and dehydration of $Zn(OH)_2$ occurred in a very narrow temperature region, corresponding TGA curves of calcium zincate showed only three distinct weight loss regions in Figure 2(a). The ratio of weight loss from 180 to 450 °C is approximately 4.025, which is in good agreement with the theoretical prediction of water loss of the composite oxides $Ca(OH)_2 \cdot 2Zn(OH)_2 \cdot 2H_2O$. Based on these facts, the chemical process during ball milling can be represented as follows:

$$Ca(OH)_2 + ZnO \xrightarrow{H_2O} Ca[Zn(OH)_3]_2 \cdot 2H_2O$$
$$\xrightarrow{>120\,h} CaZn_2(OH)_6 \cdot 2H_2O$$

3.2. *Solubility measurements*

Figure 3 compares the solubility of ZnO and $Ca[Zn(OH)_3]_2 \cdot 2H_2O$ synthesized by ball milling. It can be seen that the saturated solubility of $Ca[Zn(OH)_3]_2 \cdot 2H_2O$ is much lower than that of ZnO in 10–30 wt % KOH solutions and the maximum difference in solubility appears in 25 wt % KOH solution. Usually the alkaline electrolytes used for rechargeable zinc batteries have KOH concentration of 20–30 wt %. The low solubility of $Ca[Zn(OH)_3]_2 \cdot 2H_2O$ is undoubtedly helpful to reduce the loss of zinc ions from the anode and therefore to decrease the shape change of the electrode.

Figure 4 shows the dissolution rates of $Ca[Zn(OH)_3]_2 \cdot 2H_2O$ and $CaZn_2(OH)_6 \cdot 2H_2O$ in 20 wt % KOH solution. It is clear that both types of calcium zincate dissolve in the alkaline solution very slowly and take nearly a month to reach their saturated concentrations. These very low dissolution rates of calcium zincates imply that the shape change and dendrite formation of zinc anodes may be greatly reduced by the use of the calcium zincates as anodic active materials.

3.3. *CV features of calcium zincate*

A typical cyclic voltammogram of calcium zincate prepared by ball milling is shown in Figure 5. On the first cathodic scan, a single reduction peak appeared at −1.45 V and the position and shape of the cathodic peak were in close agreement with the electrochemical reduction of ZnO [3, 14]. The only difference in the CV curve of the cathodic of calcium zincate is that the potential is shifted by about 60 mV to negatively, indicating a

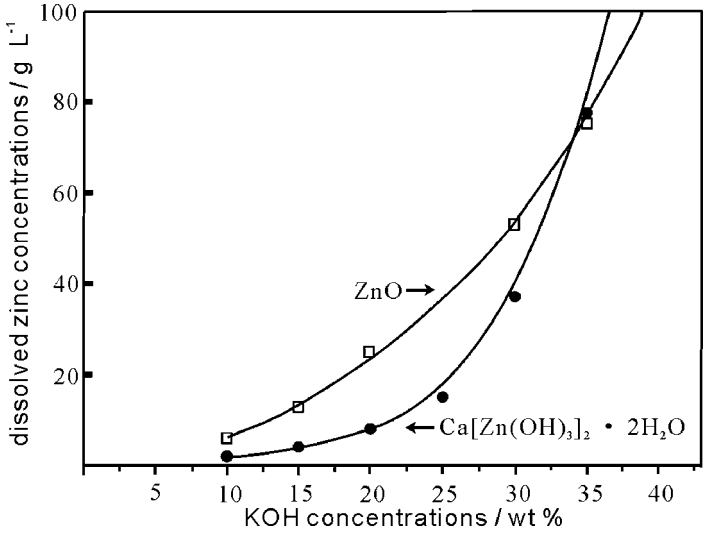

Fig. 3. Solubility of ZnO and $Ca[Zn(OH)_3]_2 \cdot 2H_2O$ in various KOH concentrations, at 298 K.

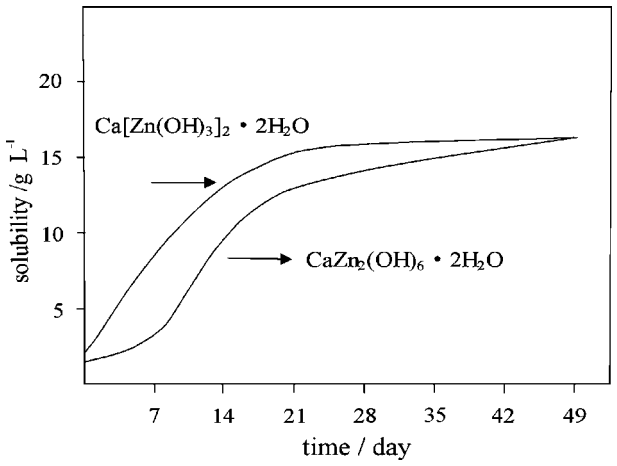

Fig. 4. Dissolution rates of $Ca[Zn(OH)_3]_2 \cdot 2H_2O$ and $CaZn_2(OH)_6 \cdot 2H_2O$ in 20 wt % KOH solution, at 298 K.

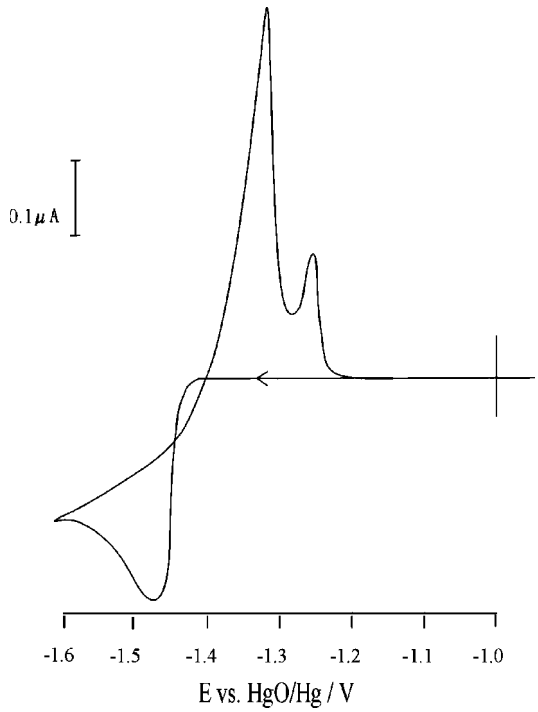

Fig. 5. First CV curve of powder microelectrode of calcium zincate in 6 mol L^{-1} KOH solution; scan rate: 1 mV s^{-1}.

stronger coordination of zinc in the calcium zincate. When the potential scan was reversed into the more positive region, two anodic peaks were observed at −1.35 and −1.28 V. The potential positions and relative intensities of the two anodic peaks were in close accordance with the CV features for anodic oxidation process of metal Zn in KOH solution [18–21]. According to the previously established model for the anodic dissolution of zinc, the two anodic peaks may be attributed to the anodic dissolution of zinc to form $Zn(OH)_4^{2-}$ and $Zn(OH)_3^-$ respectively. Thus, it seems that the existence of $Ca(OH)_2$ had no significant impact on the anodic dissolution of metallic zinc.

3.4. *Charge–discharge behaviour of calcium zincate electrode*

To characterize the cycling behaviours of calcium zincate as rechargeable anode, charge–discharge measurements were conducted on test cells using sintered Ni cathodes and with anode-limited design. Figure 6 shows the charge–discharge curves of the test cells. As expected from CV measurements, the potential profiles of the cells in charge and discharge are almost the same as observed for $Ni(OH)_2$/ZnO cells, indicating that the charge–discharge reactions of the composite oxide proceeds mainly by electrochemical deposition and dissolution of zinc. Though the discharge capacity of calcium zincate (210 mAh g^{-1}) is lower than that of ZnO, the cycleability of calcium zincate is greatly enhanced. In parallel measurements of ZnO and $Ca[Zn(OH)_3]_2 \cdot 2H_2O$ based cells, the ZnO anode worked for only a number of cycles with the appearance of severe shape change and dendrite growth, while for calcium zincate anodes, the charge–discharge capacities remained very stable.

Figure 7 shows the surface morphology of the calcium zincate electrode at the first and 80th cycles. As can be seen in Figure 7(a), the surface of the uncycled electrode shows a uniform distribution of small crystallite of calcium zincate. After 80 cycles, the surface structure of the electrode does not change much and the only change being a slightly increase in the crystallite size of calcium zincate. No shape change or dendrite growth is observed for the cycled anode of calcium zincate, suggesting that the dissolution and migration of zinc ions is effectively suppressed.

The charge–discharge mechanism of the calcium zincate electrode was characterized by XRD analysis of the reaction products after charge and discharge. Figure 8(a) shows the XRD patterns of the calcium zincate anode at 100% charge. All the XRD lines from the fully charged electrode could be assigned to $Ca(OH)_2$, ZnO and metal Zn [16]. The observation of strong XRD lines of ZnO and weak XRD signals of

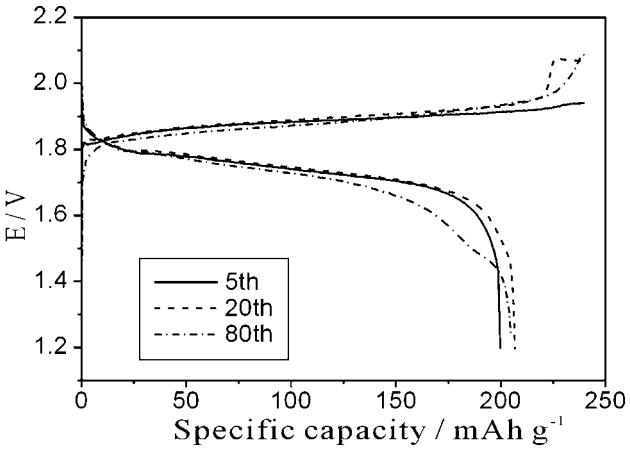

Fig. 6. Charge–discharge curves of $Ca[Zn(OH)_3]_2 \cdot 2H_2O$ based cell at various cycles: (——) 5th, (- - -) 20th and (-·-·-) 80th.

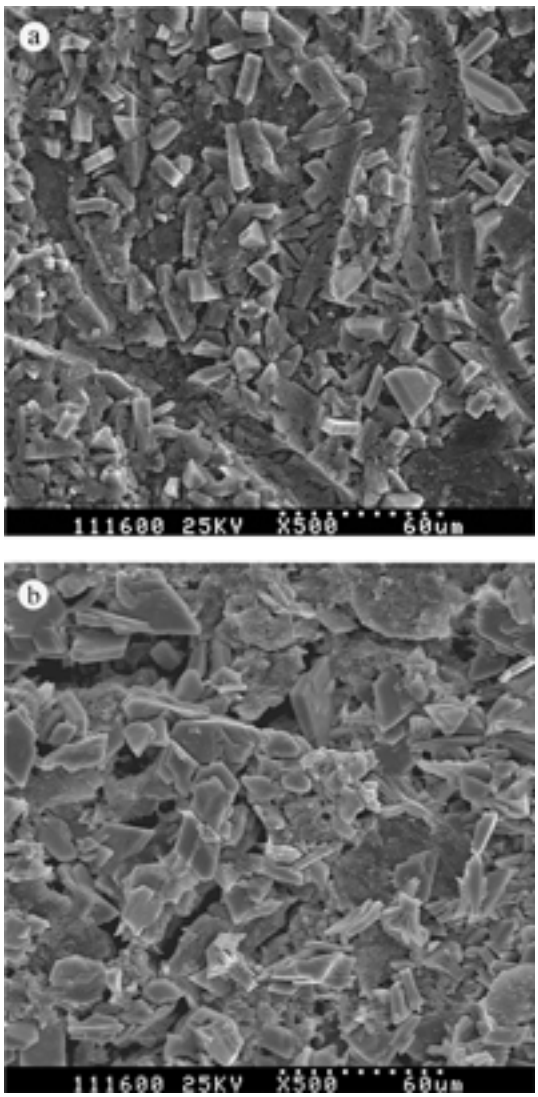

Fig. 7. SEM photographs of the surface of calcium zincate anode: (a) after first cycle and (b) after 80 cycles.

metal zinc in the charged electrode is puzzling since all the ZnO should be electrochemically reduced to elemental zinc according to the theoretical calculation of discharge capacity. This was probably due to the reaction of fresh deposited zinc with oxygen in air to form ZnO during the XRD measurements in air. A typical XRD pattern of a fully discharged calcium zincate anode is shown in Figure 9(b). Comparing the XRD lines of discharged calcium zincate anode with the pure calcium zincate, it is clear that the discharge product is mainly in the form of $Ca[Zn(OH)_3]_2 \cdot 2H_2O$. In the case of ZnO-based anodes, the discharge of metallic zinc proceeds through the formation of zincate ions at an initially stage, which undergoes a series of consecutive chemical reactions to form zinc oxide. The first step in the discharge of calcium zincate seems to take place in the same way as with the zinc oxide electrode. Subsequently, the zincate ions recombine with $Ca(OH)_2$ to form $Ca[Zn(OH)_3]_2 \cdot 2H_2O$. Based on these results, the charge–discharge mechanism of the calcium zincate anode may be described as

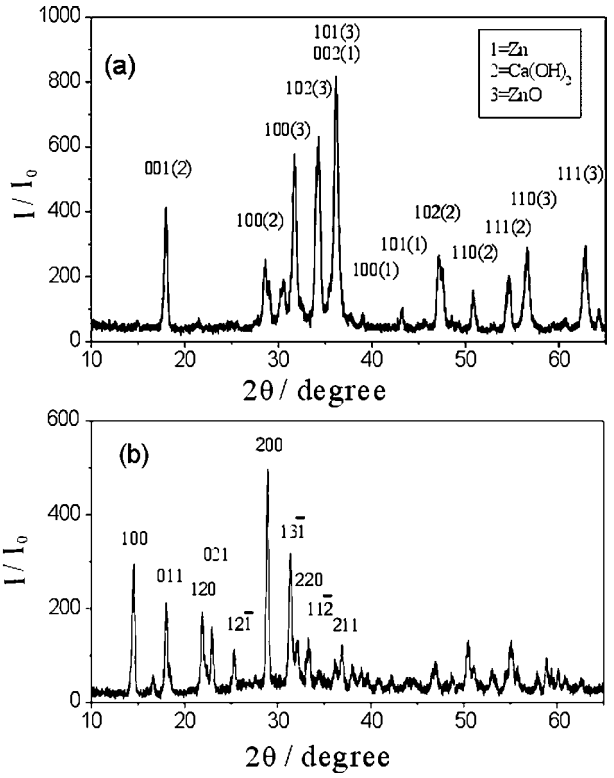

Fig. 8. X-ray diffractograms of calcium zincate anode at different state: (a) the completely charged state; (b) the completely discharged state.

$$Ca[Zn(OH)_3]_2 \cdot 2H_2O + 4e \underset{\text{discharge}}{\overset{\text{charge}}{\rightleftharpoons}} 2Zn + Ca(OH)_2 + 4OH^- + 2H_2O$$

4. Conclusion

We describe a simple method for the preparation of calcium zincate by mechanical ball-milling of ZnO and $Ca(OH)_2$ in aqueous medium at room temperature and report the structural and electrochemical properties of calcium zincate as rechargeable anodic material. The results reveal that the calcium zincate prepared by this method is more stable and less soluble in alkaline solution than ZnO-based active materials. On charge, calcium zincate is electrochemically reduced to Zn, $Ca(OH)_2$ and OH^-. During discharge, the zincate ions react immediately with $Ca(OH)_2$ to form crystalline calcium zincate. Such a charge–discharge mechanisms can avoid the loss of zincate ions from the anode, keeps the shape and structure of the anode unchanged and therefore leads to improved cycling life.

Acknowledgements

This research work was financially supported by the Special Funds for Major State Research Project of China (grant 2002CB211800) and the Chinese National High Technology Development Project (grant 2002AA323030).

References

1. C. Biegler, R.L. Deutscher, S. Fletcher, S. Hua and R. Woods, *J. Electrochem. Soc.* **130** (1983) 2303.
2. R. Jain, T.C. Adler, F.R. Mclarnon and E.J. Cairns, *J. Appl. Electrochem.* **22** (1992) 1039.
3. R. Renuka, L. Srinivasan and S. Ramamurthy, *J. Appl. Electrochem.* **31** (2001) 655.
4. J. McBreen and E. Gannon, *J. Electrochem. Soc.* **130** (1983) 1980.
5. R. Shivkumar, G.P. Kalaignan and T. Vasudevan, *J. Power Sources* **75** (1998) 90.
6. R.F. Thornton and Eric J. Carlson, *J. Electrochem. Soc.* **127** (1980) 1448.
7. G.D. Wilcox and P.J. Mitchell, *J. Power Sources* **32** (1990) 31.
8. G.D. Wilcox and P.J. Mitchell, *J. Power Sources* **28** (1989) 345.
9. J-M. Wang, L. Zhang, C. Zhang and J-Q. Zhang, *J. Power Sources* **102** (2001) 139.
10. F. Mansfeld and S. Gilman, *J. Electrochem. Soc.* **117** (1970) 588.
11. E.D. Woumfo and O. Vittori, *J. Appl. Electrochem.* **21** (1991) 77.
12. K. Bass, P.J. Mitchell and G.D. Wilcox, *J. Power Sources* **35** (1991) 333.
13. M.B. Liu, G.M. Cook and N.P. Yao, *J. Electrochem. Soc.* **129** (1982) 913.
14. J-X. Yu, H-X. Yang, X-P. Ai and X-M. Zhu, *J. Power Sources* **103** (2001) 93.
15. C-S. Cha, C-M. Li, H-X. Yang and P-F. Liu, *J. Electroanal. Chem.* **368** (1994) 368.
16. Joint Committee on Powder Diffraction Standards, 4-0733, 4-0831 and 21-1486 (1980).
17. Joint Committee [16], 25-1449 and 24-221 (1980).
18. Y.C. Chang and G. Prentice, *J. Electrochem. Soc.* **136** (1989) 3398.
19. H.J. Park and S.I. Mho, 'Analytical Sciences', 13 supplement (1997) 311.
20. M.C.H. Mckubre and D.D. Macdonald, *J. Electrochem. Soc.* **128** (1981) 524.
21. M. Cai and S.M. Park, *J. Electrochem. Soc.* **143** (1996) 2125.